J. Comp. Appl. Res. Mech. Eng. Vol. 12. No. 2, pp. 161-175, 2023 *DOI: 10.22061/JCARME.2022.7590.2010*

Journal of Computational and Applied Research in Mechanical Engineering
jcarme.sru.ac.ir
SRTTU
JCARME
ISSN: 2228-7922

Research paper

SST K-ω based air flow and heat transfer assessment in an infant incubator

D. K. Baghel*, S. L. Sinha and S. K. Dewangan

Department of Mechanical Engineering, NIT Raipur,Chattisgarh - 492010, India

Article info:

Article history:

Received: 07/12/2020
Revised: 12/09/2022
Accepted: 15/09/2022
Online: 18/09/2022

Keywords:

Incubator,
Natural convection,
Thermoregulation,
Radiation,
Turbulence.

***Corresponding author:**
devesh.baghel@gmail.com

Abstract

Neonatal incubators provide an artificial thermal environment to maintain the thermoregulation of premature babies. Several studies revealed the dry and latent heat exchange estimation between the newborn's body and the surrounding environment. Heat transfer due to convection is leading over the thermal radiation in incubators. The aim of this article is to study the airflow modeling and heat transfer coefficient over an infant's body inside the incubator. For this purpose, an experiment and a numerical simulation are carried out to develop the methodology, and subsequently computational fluid dynamics (CFD) analysis is accomplished to evaluate the heat transfer coefficient of a preterm infant. By means of the shear stress transport (SST K-ω) turbulence model, 3-D computational, models are numerically studied using the commercial CFD tool Star CCM+. Flow visualization reveals that a large-scale flow circulation pattern is produced in the mean region of the enclosed chamber, and small-scale eddies are generated at corners and close to the walls. The numerical results obtained for heat transfer assessment in the present study are validated with experimental and numerical results available in biomedical open literature.

1. Introduction

Neonatal Intensive Care Unit (NICU) is a specialized division for intense care of sick and preterm newborns. Neonates born before 36 weeks of gestation are called preterm or premature infants. The necessary growth rate of vital organs and the necessary secretion of bodily enzymes in premature babies are very faint [1]; therefore preterm infants need warm environments similar to the uterus to cope with the external environment [2]. Preterm infants need exceptional attention to cope with external physical conditions such as surrounding temperature, humidity, oxygen level, lighting beam intensity, and noise level. Incubators are electro-mechanical closed-volume devices, which provide the desired heated and humid air to newborns. Infant warming units keep the baby warm, monitor many of their vital

functions such as oxygen saturation, pulse rate, blood pressure, and support their breathing when necessary. In order to enhance the growth and survival rate of newborns, the primary goal is to maintain the thermo-neutral temperature of the infant's body [3]. In general, the desired body core temperature of newborns lies between 36.5°C - 37.5°C [4]. The infant's skin temperature is measured at the body surface while the core temperature is measured at the abdomen surface, rectum level, or under the armpit [5]. The desired thermo-neutral temperature minimizes body heat loss, which is essential to utilize nutrition in organ development and weight gain [6]. Body heat in newborn babies is produced by metabolic and non-shivering thermogenesis. Metabolism accomplishes the total energy requirement that the supports maintenance, repair, and growth of an infant [7]. Poor metabolic rate and a greater ratio of body surface area to body mass are prone to excess heat loss in low-birth-weight babies; which lead to hypothermia, so incubators are preferred in such critical care conditions [8]. In incubators, heat transfer due to convection, is the source of heat gain and radiation is the cause of major heat loss; while this phenomenon is the opposite in radiant warmers. Neonates lose body heat by means of dry heat loss (by radiation 39%, convection 34%, and conduction 3%) and latent heat loss (by combined skin evaporation and respiration process 24%) [9].

In a numerical study, Yamaguchi *et al.* [10] demonstrated the transient flow mixing phenomenon and unstable temperature distribution inside an incubator. In a numerical simulation, Ginalski *et al.* [11] incorporated an infant heat balance module (IHBM) as a supplementary model to explore the mass transfer mechanism. This model is numerically verified and capable to evaluate the evaporative losses from infant skin under various operating conditions. Kim *et al.* [12] verified the non-uniform airflow velocity inside an incubator using hot-wire anemometer measurement method. Moreover, the usage of an overhead screen in double wall infant incubator significantly lowers the radiation heat loss; as a result of which the infant's skin mean temperature is raised by 2 °C, thus avoiding the risk of hypothermia [13]. Temperature distribution, relative humidity, and oxygen content inside the incubator is strongly influenced by the ventilation arrangement system. In previous studies (Ganesh *et al.* [14-15]), it is found that: the change in the inlet ventilation conditions changes the indoor thermal conditions, and the presence of occupants also precisely affects the flow and heat characteristics of the indoor environment. In the case of an isothermal enclosed channel, fluid velocity reduction and flow reversal are obtained close to the wall [16]. In enclosed volume, Eckert number increment leads to higher steady state temperature distribution in the flow domain [17]. Several studies reveal that ventilating patterns, i.e., location of inlet and outlet ports, dimension of ports and position (axial, longitudinal) etc. have significant effect on flow and heat transfer characteristics inside incubator.

To date, most of the studies on the physical processes occurring inside incubators have been carried out using experimental and numerical techniques. Majorly heat transfer in the incubator is due to convection; thus, in the present study metabolic heat production and heat loss due to moisture transport have not been taken into account.

2. Numerical methodology

The present study incorporates an experimental visualization and numerical analysis of flow and heat transfer in an enclosed volume. Flow and thermal field due to the turbulent convective environment inside the incubator have been analyzed. The present work is a case of a single-phase turbulent flow and heat transfer model which is governed by a steady 3-dimensional form of the continuity equation, time-averaged incompressible Navier-Stokes equations, and energy equation. Additional scalar transport model for turbulent flow and radiation transport model for angular discretization of the radiation spectrum is incorporated into the present study. Basic governing equations can be referred to from references [18, 19].

There is no mechanical heating unit inside the incubator; therefore, in order to enhance the

convective heat, transfer the airflow is kept relatively low. Convective flow pattern, whether natural or forced, is identified by the relation between internal flow characteristics such as viscous forces, inertial forces, gravitational forces, and relevant diffusivity parameters. The non-dimensional numbers presented by Eqs. (1-4) describe the flow characteristics as follows:

Reynolds number $$Re = \frac{\rho V D}{\mu} \quad (1)$$

Grashof number $$Gr = \frac{g\beta \triangle T L^3}{\nu^2} \quad (2)$$

Rayleigh number $$Ra = Gr * Pr \quad (3)$$

Prandtl number $$Pr = \nu/\alpha \quad (4)$$

where ρ (kg/m^3) is the density of air, V (m/s) is the velocity, D (m) is the hydraulic diameter of inlet jet, μ (kg/m-s) is the dynamic viscosity, g (m/s^2) is the acceleration due to gravity, β (K^{-1}) is the coefficient of thermal expansion, △T (K) is the temperature gradient, L (m) is characteristic length, ν (m^2/s) is the kinematic viscosity or momentum diffusivity, and α (m^2/s) is the thermal diffusivity of air.

The ratio of the non-dimensional number Gr/Re^2 is calculated to verify the nature of the flow; i.e., natural or forced convection. For all the enclosed volume models, this ratio is greater than 1 in all cases, i.e., flow occurs due to natural convection inside the test chamber and incubator. Rayleigh number is also in order of greater than 1.0×10^6; i.e., a higher Ra number resembles the flow turbulent in nature, thus airflow in the computational domain is solved with the turbulence model. The ratio of these non-dimensional numbers is presented in Table 1, as follows:

Table 1. Non-dimensional number of enclosed volumes.

Model	Ra	Gr/Re^2
Experimental test model	1.3×10^6	1.75
Experimental numerical model	1.5×10^6	2.04
Incubator CFD model	3.7×10^7	4.74

3. Methods

The driving mechanism of indoor airflow is complex. The fluid motion does not hold a well-structured pattern in any ventilation system. In such systems, indoor airflow analysis, temperature distributions, heat transfer, humidity distribution, draft conditions, etc. are calculated as per the design and system requirement. The present paper incorporates an experimental study followed by a numerical analysis of airflow and heat transfer in an infant incubator.

3.1. The experimental model

Airflow inside the incubator is a spatial and temporal superposition of natural and forced convection. In order to validate the flow phenomenon inside the incubator, initially the flow study is carried out in an experimental chamber. Fig. 1 and Fig. 2 [20] represent the experimental chamber model for the purpose of this investigative study. The dimensional aspect of the closed chamber is taken as 1.2 m × 0.8 m × 0.6 m (length × width × height, respectively).

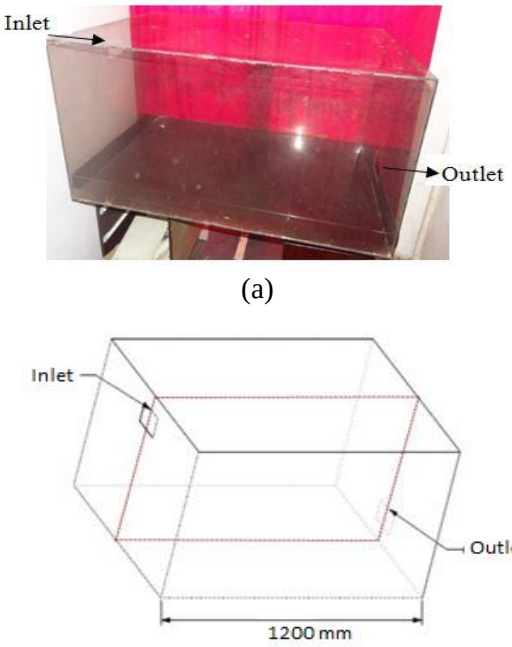

Fig. 1. (a) Experimental test chamber [20] and (b) schematic of test chamber geometry.

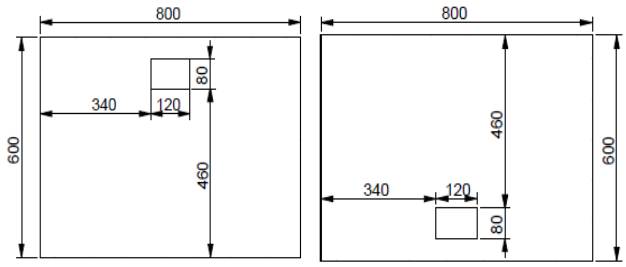

Fig. 2. Dimension (in mm) of experimental model: (a) inlet side wall and (b) outlet side wall.

The unidirectional airflow at the entrance of the enclosed chamber has been achieved using a duct. Air enters the enclosed chamber through the duct via inlet vent and exits through the outlet vent, which has been provided at the opposite end as shown in Fig. 1. A thermal anemometer is used to measure airflow velocity during the experiment. A slot of 100 cm × 3 cm is formed at the ceiling and floor of the model to adapt the strip of similar dimension. Small holes with a diameter of 6 mm are created at a distance of every 15 cm. Air velocity is measured using a thermal anemometer by inserting its sensor probe through a hole; at the same time, other small holes are closed with a tape to prevent air leakage. The detailed drawing of the test model is shown in Fig. 2.

3.1.1. Flow visualization

The smoke visualization method has been adopted for the flow pattern observations. Air charged with vaporized kerosene smoke/mist is illuminated by two flashlights mounted inside a reflective hood placed above the small closed and ventilated room. The scattering of smoke particles by airflow has been captured by using a fixed camera. It took 3 hours to stabilize the flow field, and then air velocity measurement and smoke concentration visualization were captured. The lighting system of high-intensity light is used in the experiment. Capturing the motion of the dispersed light due to smoke movement is the basis of smoke visualization. The airflow within the chamber is supplied by a fan. In order to supply unidirectional flow and the required quantity of flow without losing heat to the external environment, a 1.5 m long insulated duct is used.

Acrylic glasses are highly reflective; therefore, visualization of the airflow inside the acrylic glass is complicated. Also, greater reflectivity interrupts capturing the flow pattern images. The smoke visualization method is mostly used to capture the convective flow pattern. Vapor is injected into the flow for better visualization. The vapor follows the line of filaments (lines consisting of all the particles of fluid passing through the injection point). In regular flow, filament lines represent the lines tangential to the velocity vector, everywhere. Hence the smoke flow visualization reveals the entire flow diagram in and around a body. Ideally, the density of smoke particles should be similar to the fluid. If the density of the fluids is different, the path followed by fluid and smoke may significantly differ due to their gravitational and inertial forces. Density of smoke is slightly higher than air, therefore it moves outward if the current lines are curved and at lower velocity the smoke descends significantly under the action of gravity. These effects are negligible when flow maintains enough momentum in the domain. In laminar flow, smoke filament remains well defined but quick diffusion occurs in a turbulent flow. The best results are obtained at a low velocity.

3.2. Computational model

CFD methods are used in the forecast of scalar quantity and other complex flow phenomena such as turbulence mixing, heat exchange, particle tracking, etc. within the computational domain. In the present study, numerical simulation is carried out in an experimental as well as a simplified incubator model. Followings are the basic assumptions made for both models:

- Air flow is in steady state condition;
- Heat loss due to moisture transport is neglected.
- Physical properties of air (incompressible gas) are constant throughout the analysis.
- Flow field is analyzed with the presence of turbulence. Small vertices in close proximity to the infant's skin interfere with evaporation and convection heat losses; thus, *k*-ω SST (shear-stress transport) turbulence model is used.
- All y+ wall treatment is used to resolve the viscous effects in close proximity of the wall.

3.2.1. Numerical model of an experimental chamber

Fig. 3(a, b) demonstrates the computational model of the test chamber. Full-length duct at the inlet side is not considered in the simulation. In order to achieve fully developed flow at the entrance of the chamber and to avoid recirculation at the exit of the chamber, the inlet and outlet are reasonably extended to 1000 mm and 500 mm, respectively as shown in Fig. 3(b). The finite volume method with ≈2.6 million polyhedral cells is used in numerical simulation.

In the present model, the computational domain is consisting of test chamber volume and inlet/outlet sections. The experiment has been done at various airflow rates between 10 L/min to 50 L/min. The exit face is considered as the pressure outlet to atmospheric pressure (gauge pressure of 0 Pa). Airflow encounters the diffusion and recirculation at inlet and outlet zone inside the chambers, respectively.

Such phenomenon leads to significant gradient in scalar parameters within the core region of the flow. Thus, in order to validate the flow pattern in both the numerical and experimental models, two straight lines (line 1 and line 2) have been considered to measure air velocity following through inlet and outlet section of the domain.

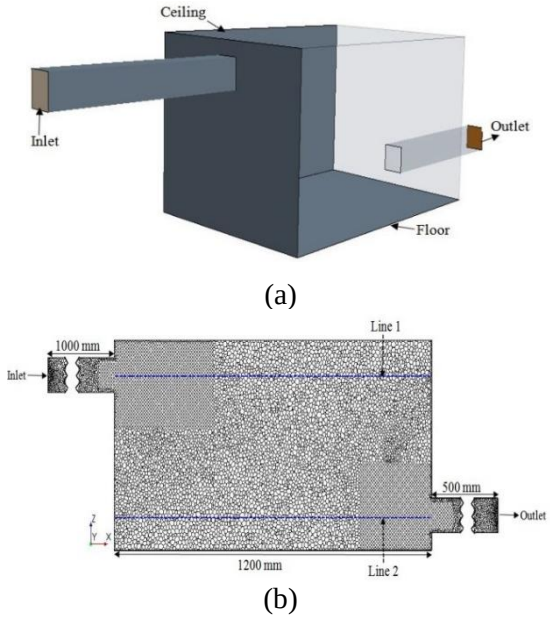

Fig. 3. Computational model of test chamber; (a) CAD model and (b) mesh at mid-section.

Line 1 is drawn from the center of the entrance to the opposite wall and similarly line 2 is drawn from the center of the exit section to the end of the opposite wall. Both lines are parallel to the ground as shown in Fig. 3(b).

3.2.2. Validation of test chamber model

As shown in Fig. 4, non-dimensional velocity at the desired line probe location was computed and compared against the measured experimental data. Good agreement has been found between all the variations of k–ω model and experimental measurement. In the captions of Fig. 4, the "standard k–ω:1" refers to standard k–ω model (with all y+ wall treatment), the "standard k–ω:2" refers to standard k–ω model (with low y+ wall treatment) and " SST k–ω" refers to the SST k–ω turbulence model. It is observed that non-dimensional velocity trend is sensible and similar to the results obtained in the experimental study.

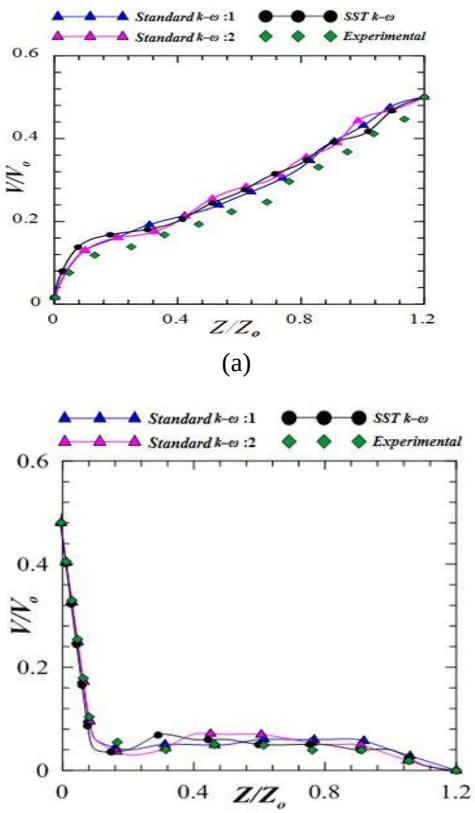

Fig. 4. Dimensionless velocity comparison at the desired line probe location (a) along line 1 and (b) along line 2.

The density of smoke used in the experimental study is slightly higher than the air modeled in numerical simulation. Thus, localized air velocity in free stream zones is predicted greater than the experimental results. As shown in Fig. 4(a) and Fig. 5, air flows into the chamber at a higher momentum, thus velocity plotted against line 1 is increasing along the length of the chamber.

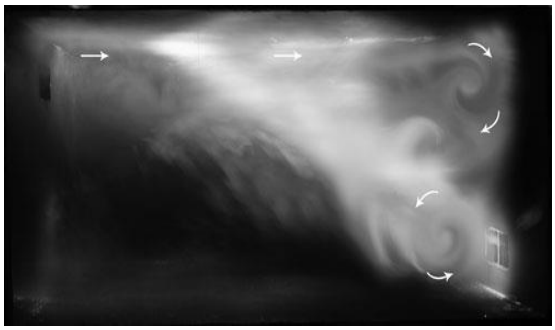

Fig. 5. Airflow pattern in the experimental visualization.

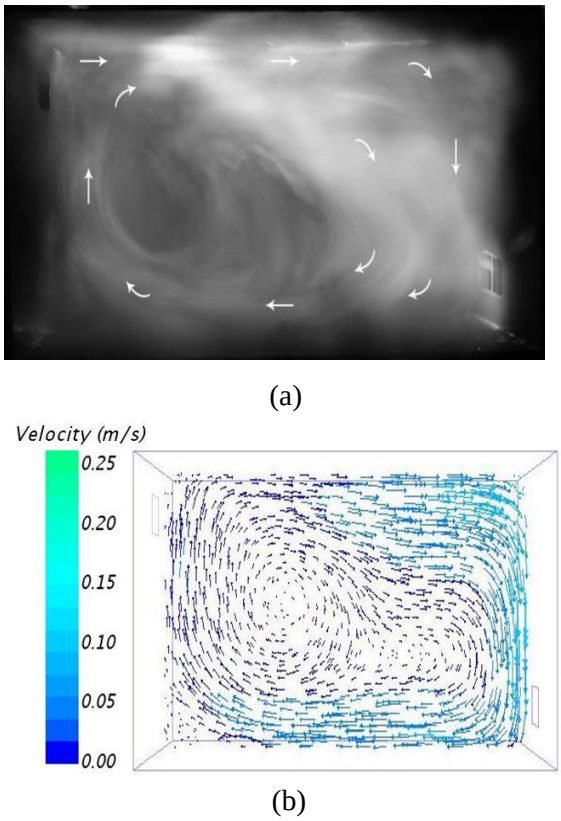

(a)

(b)

Fig. 6. Flow field comparison between (a) experimental visualization and (b) CFD result.

Flow recirculation towards the outlet zone extracts the mean flow energy and lowers the air velocity along line 2. The density variation results in a higher velocity of air at all points in the measurement lines as shown in Fig. 4(b) and Fig. 6(a, b).

As shown in Fig. 5, the mainstream flow is attached to the ceiling (top surface) and strikes the opposite end wall. On the right top corner, eddy formation is observed due to repulsion and a change in the momentum of flow. Chaotic motion leads to irregularity in the mean flow regime. The stagnant zone is observed under the entry part. There are two recirculation zones that have been formed and can be easily viewed, one in the upper right corner and the second in the right bottom corner near the exit.

Results obtained from simulation and experimental smoke visualization have been compared in Fig. 6(a, b), which reveal the similarity between the two cases to a large extent. There is an air stagnation pocket in the lower-left corner which is observable in both the experimental and simulation results. The mainstream of the airflow from the entrance is attached to the ceiling, strikes onto the opposite wall and descends. A large-scale flow recirculation region is formed, which is illustrated by arrows in experimental visualization results shown in Fig. 6(a). Enhanced mixing of the flow tends to reduce the rotational pattern as shown in Fig. 6.

Establishing a three-dimensional flow in a closed enclosure is very complicated. Further improvements are needed in the design of conduits and flow straighteners. The jets are inherently unstable, and the smoke examined is wavy. It is estimated that the capacity of a smoke generator was not enough to precisely capture the recirculation cells. The tests could only be carried out at very low input air velocity because, at a higher velocity. The dispersion of the smoke was so rapid that even with the naked eye, no idea could be obtained on the flow field. Thus, measurement lines (line 1 and line 2) have been considered to investigate the nature and momentum of the fluid inside the chamber. Therefore, only a limited number of results were presented. Results of SST k–ω turbulence model have demonstrated a fair correlation with the experimental results.

3.2.3. Numerical model of an infant incubator

Precise modeling of the incubator is relatively complex; therefore, in the current study, a simplified incubator model is considered. A stable three-dimensional airflow modeling is done in a simplified model. The computational domain consists of an infant manikin, inlet, outlet, mattress, hood frame, and cabinet base as shown in Fig. 7(a). Fig. 7(b) corresponding to the geometrical dimension of Baby Nest I-plus incubator [21]. The dimension of the incubator model is considered as 0.85 m × 0.53 m × 0.49 m (length × width × height, respectively). The hood section maintained in the simulation model is as per product specification. The Incubator hood thickness is considered 2.5 mm. The computational domain is considered the half-symmetrical model. In order to monitor scalar parameters, several sectional planes at the infant's anterior (calf, thigh, abdomen, chest, and forehead) are considered.

Geometry of neonate model with various body segments, i.e., head, trunk, arms and leg, is designed in CAD package using NX-Unigraphics. The height and total surface area of the infant is considered as 0.43 m and 0.1545 m^2, respectively and the exposed surface area of the infant is considered as 0.133 m^2 [12, 22]. Dirichlet boundary condition is applied at the infant's skin by varying skin temperature between 33.5°C to 36.5°C for the anterior body segments [23]. Premature babies are feeble and always in a growing phase, thus the emissivity of infant skin is ranging from 0.95 to 0.98. In the present study, the emissivity of the infant's surface is considered as 0.95 [4].

Cabinet frame is modeled as solid plastic (PVC) body and thermo physical properties of the incubator frame material are shown in Table 2. Mattresses are manufactured of low thermal conductivity foam (latex, memory foam, etc.) materials. 'The upper and side faces of the mattress are exposed to ambient air; thus, conjugate heat transfer takes place at the interface between the mattress surface and air. Mattress dimension is considered as 0.8 m × 0.48 m × 0.03 m (length × width × thickness, respectively). Low thermal conductivity material works as an insulator; thus, the mattress thermal conductivity and emissivity is considered as 0.03 W/m·K and 0.9, respectively [4]. Air is supplied with a uniform flow rate of 50 L/min at 29°C [23]. Two inlet and outlet slots are defined in the transverse and longitudinal direction in the axis to the neonate, inside the incubator, respectively, as shown in Fig. 7(a).

Fig. 8(a) represents the meshed model of an infant in a spine-relaxed position and Fig. 8(b) represents the line probes to quantify the velocity components around the infant's anterior surface. As shown in Fig. 8(b), a small channel is introduced into the present model for an air inlet rather than a conventional inlet opening. Two inlet and outlet slots are defined in the transverse and longitudinal direction in the axis to the neonate inside the incubator, respectively as shown in Fig. 7(a).

Inlet channel side walls and cabinet base surface are defined as an adiabatic wall. The interior surface of the cabinet frame works as an interface between the air domain and solid zone.

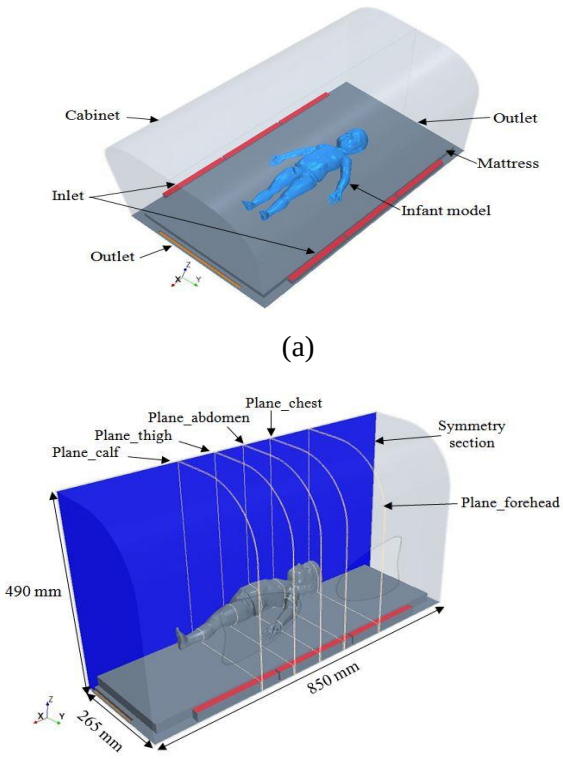

Fig. 7. (a) Infant incubator model and (b) incubator dimension with sectional plane.

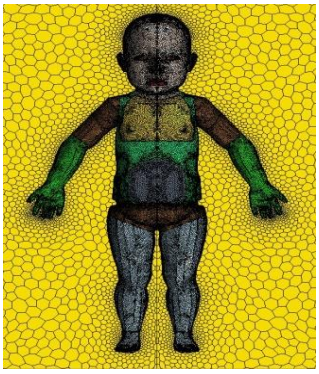

(a)

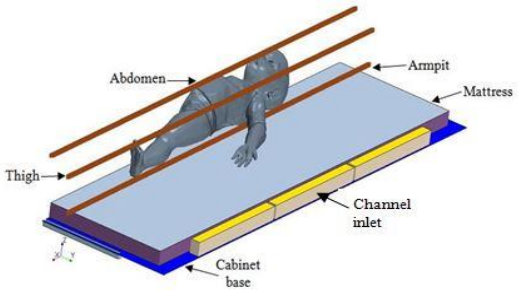

(b)

Fig. 8. (a) Infant mesh model and (b) line probe at infant anterior.

The exterior face of the cabinet frame\hood is exposed to the environment, to dissipate and radiate heat to the atmosphere. At a steady state condition, the interior surface of the hood\frame closely attains the relative mean temperature of the incubator volume; thus, the present study focused on the flow field development and heat transfer due to the natural convection inside of the incubator. Metabolic heat production, evaporative heat loss and thermal radiation are not modeled in the present study.

Table 2. Thermophysical properties

Properties	Air [24]	Cabinet [11]	Mattress [4]
Density (kg/m^3)	1.168	1700	55
Specific heat (J/kg-K)	1007	1400	2996
Thermal conductivity (W/m-K)	0.02568	0.14	0.06
Dynamic viscosity (Kg/m-s)	1.598×10^{-5}	-	-
Emissivity	-	0.9	0.9
Expansion coefficient	0.003245	-	-

3.3. Mesh sensitivity analysis

Numerical analysis is carried out on various mesh model to estimate the grid convergence index (GCI) related to grid sensitivity analysis proposed by Celik *et al.* [25]. Average velocity at line probe at inlet side and surface average heat flux at infant's skin is considered for the grid sensitivity analysis. According to grid sensitivity analysis, the GCI for most refined element sets is in order of 1.6 % and 0.6 % for the experimental and incubator model, respectively.

The test chamber model is meshed with ≈2.6 million cells. Due to symmetry in nature, a half-symmetrical computational domain of the incubator is discretized with ≈1.5 million polyhedral cells for numerical analysis.

Moreover, Fig. 9 represents the results of grid sensitivity analysis for average velocity (test chamber model) at line-1 and area weighted average total heat flux at the infant's skin surface. It is evident that there is no significant change in results achieved on the 5th iteration; hence results are presented from the 5th iteration case.

4. Results and discussion

A steady-state simulation with second-order convective scheme is carried out using Star CCM+ for the experimental and incubator models. Numerical results obtained in the incubator model are compared with results reported in open literature. Emphasis has been placed on the local refinement of mesh around the infant's skin to capture the flow structure Fig. 8(a). Also, the non-dimensional distance of the first cell at the walls is maintained at a threshold of 0.01≤ Y+ < 1 at the infant's skin surface.

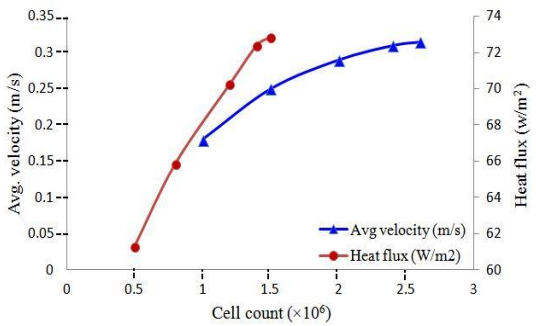

Fig. 9. Mesh sensitivity analysis.

4.1. Steady state analysis

Initially, steady state airflow and heat transfer analysis is carried out in the infant incubator. Several studies reveal that the flows in incubators are transient in nature and transition to unsteadiness is observed in the current study as well. In an incubator, operating conditions, infant's anterior structure, shape of incubators etc. strongly affect the flow and temperature field around the neonates. Natural convection is unsteady in nature; thus, wavering in flow and temperature distribution exists.

Fig. 10 illustrates the velocity contour at infant's anterior transverse plane sections, i.e., forehead, chest, abdomen, thigh and calf. Small vortices are formed close to the ears and large-scale flow circulation is altered towards the side wall. Large-scale vortices are developed in core zone. Local velocity at the chest is greater than 0.1 m/s, which carries heat away from body surface and lowers the infant's body temperature at trunk area. Counter-rotating vortices are developed between abdomen and arm, on both sides. These low velocity rotating eddies are stagnant and reduce the convective heat loss to surrounding. A swift flow is observed at the thigh section. Large and small rotating vortices are formed on upper body and under the thigh, respectively. At calf section, small vortices are formed between both the legs and air flows towards the mattress upper surface with velocity < 0.03 m/s. Moreover, flow circulation pattern breaks up due to the mixing of flow steams and moves towards outlets.

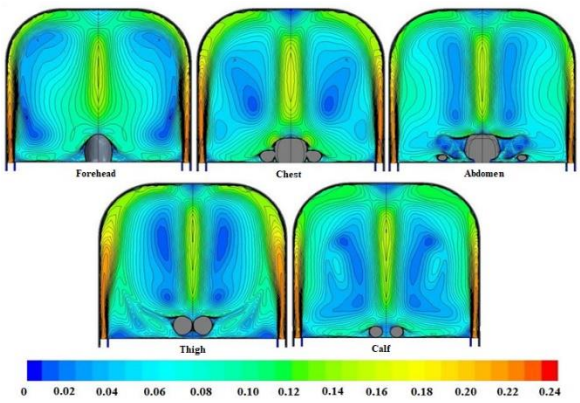

Fig. 10. Velocity contour at infant anterior section.

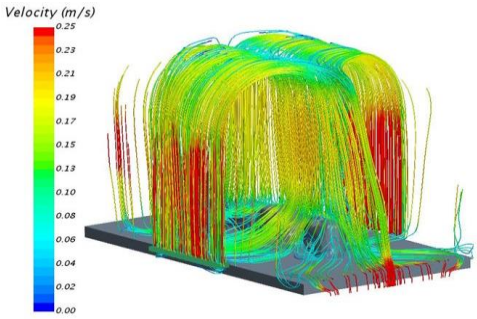

(a)

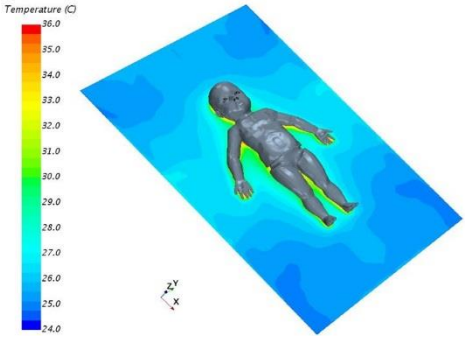

(b)

Fig. 11. (a) Velocity streamlines and (b) temperature distribution on mattress surface.

As shown in Fig. 11(a), the main flow stream from the inlet is divided into two separate streams. Flow streams from inlets are attached to the side walls and warm up the interior screen. The flow stream at the central zone in the incubator is kept on circulating, mixing, and warming up the infant. Another flow stream, after mixing and momentum exchange to the mainstream flow, travels to the outlets.

Temperature distribution on mattress upper surface is shown in Fig. 11(b). The temperature of the infant and the inlet air is greater than the mattress which is kept at room temperature. This temperature gradient causes heat exchange due to convection and radiation, thus temperature on the upper surface of the mattress near the infant is uneven and greater than the surrounding temperature.

Fig. 12 illustrates the temperature variation of line probes along the infant's longitudinal direction. These line probes, as shown in Fig. 8(b), are in close vicinity to skin where small eddies are formed.

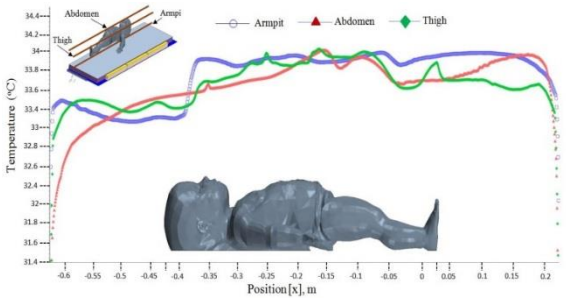

Fig. 12. Temperature variation at infant anterior line probe.

The distance of line probe from skin surface is varying from 5 - 7 mm due to irregularity in body shape. Small-scale eddies formed under the armpit, head and neck are stagnant, which locally increase the temperature around the body. Thus, line probe passing through the armpit shows significant increment in the temperature at the forehead onwards. Line probe refers to abdomen is passing through the center of the computational domain. The cross mixing of the flow increases the temperature from the head to the abdomen and then fluctuating towards the calf. Enhanced mixing increases the air temperature and keep it warm towards the outlet.

Fig. 13(a-c) represents comparisons of axial velocity between experimental and numerical results, computed at 2 mm away normal to the infant's anterior surface. Velocity components i, j and k refer to velocity in x, y and z direction and magnitudes are presented as u, v and w, respectively. v-velocity is significantly higher than u and w. In order to establish the solution method, air is supplied at a higher flow rate similar to the experimental study carried out by Kim *et al.* [12].

As shown in Fig. 13(a), the u-velocity component in the present study is reasonably higher than the numerical results presented in the literature. This is due to the fact that; in the literature model inlet and outlet are placed in the transverse direction, whereas in the present model outlet is in the longitudinal direction which enhances the velocity in the x direction. Moreover, velocity movement is similar to the experimental results.

As shown in Fig. 13(b), v-velocity is decreasing from the forehead to the chest and subsequently increases till the foot. At the central zone, the opposite stream flow cancels out the momentum, therefore, air velocity reduces from the head to the abdomen. There is a noticeable difference in velocity magnitude but the pattern is quite similar to the results obtained in the literature model [12].

As shown in Fig. 13 (c), velocity variation in the present result is in blend of numerical and experimental results obtained in the literature. w-velocity is irregular from the forehead to the thigh. Velocity pattern from the abdomen to the foot is similar in the present and literature numerical model. Rounded square cross section of the upper hood directed the high intensity flow towards the infant's body, but flow separation at the infant's skin and directional change lowers the magnitude of w-velocity component.

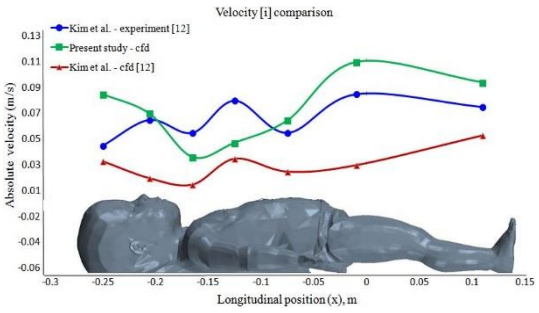

(a)

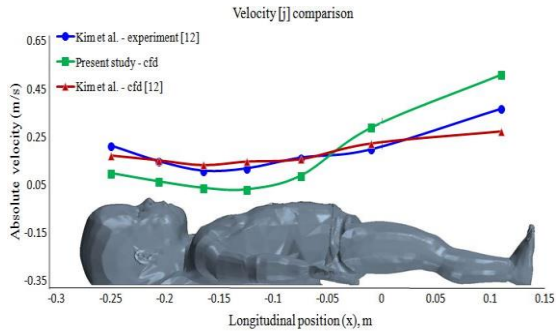

(b)

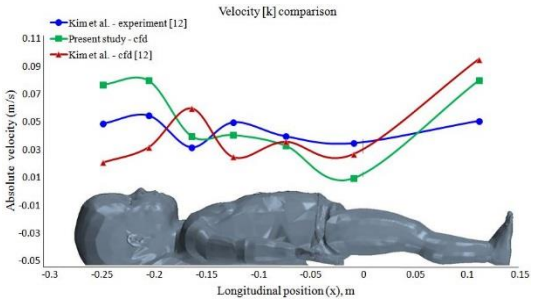

(c)

Fig. 13. (a) u-velocity at infant anterior parts, (b) v-velocity at infant anterior parts and (c) w-velocity at infant anterior parts.

Fig. 14(a, b) represents the temperature contour on transverse and longitudinal (symmetry) plane section at the trunk. The temperature gradient between the infant's skin and air leads to ascending motion of air which reflects the qualitative nature of natural convection. Enhanced mixing generates recirculation flow pattern as expressed in Fig. 10. This leads to uneven temperature distribution on both sides of the trunk as shown Fig. 14(a). Convective and radiative heat transfer due to temperature gradient between the infant's skin and surroundings (air and the interior surface of incubator wall) causes localized airflow movement around the infant's body. As shown in Fig. 14(b), air in the vicinity of the infant's skin is warmed up due to radiative heat transfer from infant skin. This warm air moves upward due to the density gradient and heat dissipation is carried out by free convection phenomenon.

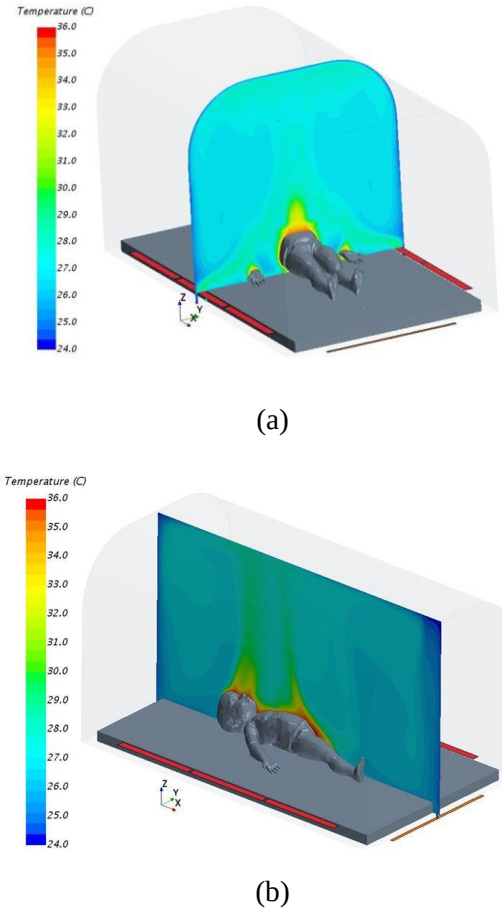

Fig. 14. Temperature contour at (a) transverse section and (b) at longitudinal section.

Convection and radiation heat flux distribution on preterm infant's skin is shown in Fig. 15(a, b). A positive sign denotes heat gain to skin surface while a negative sign means heat loss from the infant's skin to the ambient air. It is observed that the upper head of the trunk imparts the highest heat gain followed by face and arm while sides of the leg and the chest shows energy loss to the environment due to convection as shown in Fig. 15(a). As shown in Fig. 15(b), head losses highest radiant energy followed by the trunk and legs. Also, radiative fluxes are uniformly distributed on the trunk and legs. The dead and the chest are imposed to the higher temperature. Cross flow mixing from the inlet occurs at the central zone of the incubator, i.e., convective heat transfer is flow dominant over the chest and the trunk. The maximum value of the convection and radiation heat loss is observed for the trunk and the head, are 27 W/m^2 and 60 W/m^2, respectively.

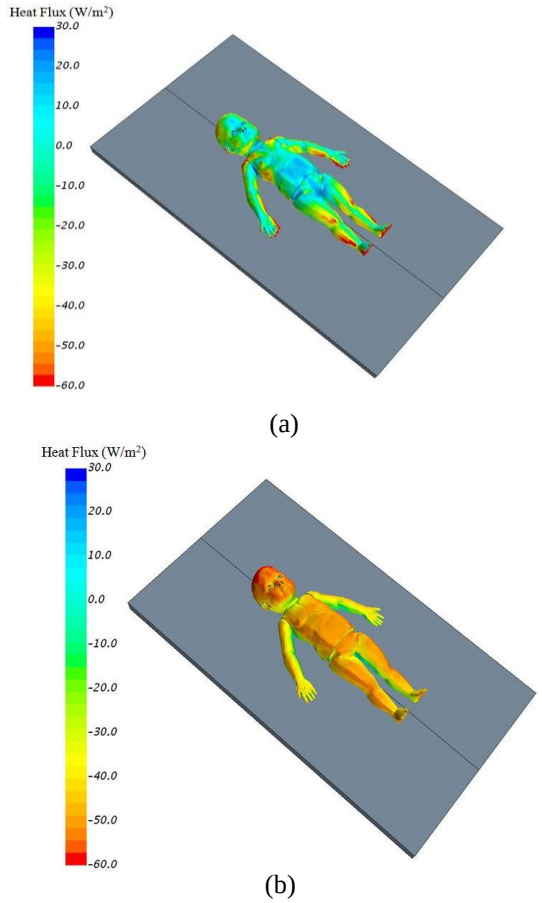

Fig. 15. (a) Convection heat flux distribution and (b) radiation heat flux distribution.

4.2. Heat transfer coefficient correlation

As the inlet air temperature increases, heat loss from the infant's skin decreases. This section illustrates the estimation of convection and radiation heat transfer coefficient for the infant's skin using Newton's law of cooling and Stephan-Boltzmann equation, respectively as follows:

$$q_{conv} = h_{conv} A_{skin} (T_{skin} - \overline{T_a}) \quad (5)$$

$$q_{rad} = h_{rad} A_{skin} (T_{skin} - T_r) \quad (6)$$

where A_{skin} and T_{skin} are the respective infant's body surface area and the area weighted skin temperature. $\overline{T_a}$ is air bulk temperature inside the incubator. T_r is the radiant temperature. T_r is a derived quantity and depends upon the incubator air temperature, room temperature and radiation properties of the incubator cabinet frame\hood material. Decima *et al.* [22] proposed an empirical correlation for estimation of the radiant temperature inside the incubator and it is applicable for the room temperature ranging between 23°C to 25°C, as follows:

$$T_r = 0.724(T_{in} - 31.93) + 29 \quad (7)$$

where T_{in} is the incubator's inlet air temperature.

Results obtained in the present study for radiation and convection heat transfer coefficient are compared with the experimental and numerical results available in the open literature. The manikin structure and incubator shapes are different in reported studies. Also, segment-wise exposed areas of the infant's anterior body parts are significantly different from each other in considered reference studies. Hence, marginal but precise differences have been observed in compared results.

Heat transfer coefficient of the whole body obtained in the present study is shown in Fig. 16(a, b). Results gained are in qualitative agreement with the open literature results [7, 9, 22, 23, 26] with minor differences.

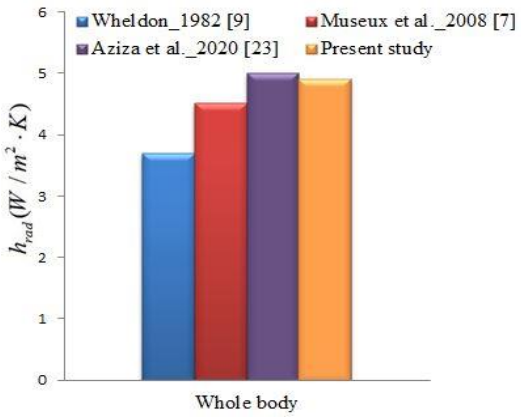

(a)

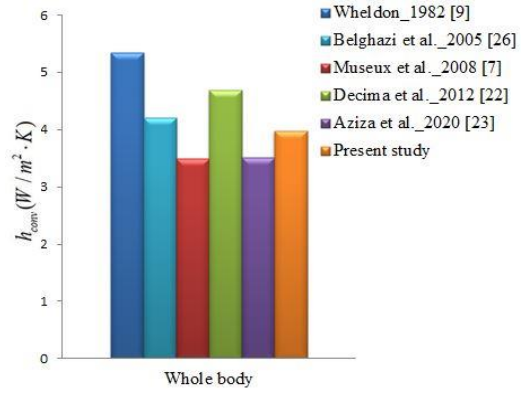

(b)

Fig. 16. (a) Radiative heat transfer coefficient for whole body and (b) convective heat transfer coefficient for whole body.

This is due to the fact that there is relative variation in incubator geometry, infant anterior body structure, and infant uncovered surface area as well as geometrical configuration of the infant. Convective and radiative heat loss from the infant's skin is obtained as 2.3 W and 2.81 W, respectively.

5. Conclusions

The present work is aimed to study and evaluate the flow and heat exchange phenomena using appropriate SST k-ω turbulent model. Results obtained in experimental and numerical studies for the enclosed chamber illustrates the similarity in formation of large-scale rotating flow structure. Numerical results show that non-dimensional velocity measured along the line probe are in fair agreement with the experimental results.

A marginal difference is noticed in segregated flow velocity inside the incubator when the present results are compared with the experimental results reported by Kim *et al.* (2002). This is particularly due to the relative difference in size and geometry of the infant, and the incubator model. The absolute velocity pattern in the present study is quite similar to the experimental results available in the literature. Numerical results show sensibly uniform radiant flux distribution on the trunk and leg of the neonate. Head imparts greater radiation heat loss than other body parts. Trunk gains highest convective heat than the other body parts. Convective and radiative heat transfer coefficients obtained in current study are in order of 3.95 W/m^2 and 4.9 W/m^2, respectively. Heat transfer coefficients are compared and showed that convective and radiative heat transfer coefficient is varying by 12.3% to 34.4% and 2% to 24.5%, respectively. Velocity and temperature field within the incubator depends upon various parameters such as shape and dimension of the incubator, incubator hood cross section (oval, wedge, rectangular, semi-circular etc.), infant's anterior structure, air flow rate, location of the inlet and outlet ports, etc. These factors manage the air velocity and heat exchange between the body and the environment, thus numerical models including metabolic heat production and moisture transport modeling can be further assessed to estimate the evaporative heat transfer coefficient.

Acknowledgment

The authors would like to thank Mechanical Engineering Department, NIT Raipur, and Dr. Tikendranath Verma for accessing the experimental setup related to his Ph.D. dissertation, to be used in the present research work.

References

[1] R. E. Black, S. Cousens, H. L. Johnson, J. E. Lawn, I. Rudan and D. G. Bassani, "Global, regional, and national causes of child mortality in 2008: a systematic analysis", *Lancet*, Vol. 375, No. 9760, pp. 1969–1987, (2010).

[2] N. Charpak, J. G. Ruiz Pelaez, Y. Charpak and R. martinez, "Kangaroo mother program: an alternative way of caring for low birth weight infants? One year mortality in a two cohort study", *J. Pediatrics*, Vol. 94, No. 6, pp. 804–810, (1994).

[3] A. Lyon, "Applied physiology: temperature control in the new born infant", *Current Paediatrics*, Vol. 16, No. 6, pp. 386–392, (2006).

[4] D. K. Baghel, S. L. Sinha and S. K. Dewangan, "Numerical analysis of heat transfer under a radiant warmer", *Heat Transfer*, Vol. 49, No. 4, pp. 2406-2421, (2020).

[5] J. Takayama, W. Teng, J. Uyemoto, T. Newman and R. Pantel, "Body temperature of newborns: what is normal", *Clin. Pediatr (Phila)*, Vol. 39, No. 9, pp. 503-510, (2000).

[6] G. Boxwell, *Neonatal Intensive Care Nursing*, 3rd ed., Taylor & Francis Group, UK, ISBN 9780203186145, (2019).

[7] N. Museux, V. Cardot, V. Bach, S. Delanaud, L. Degrugilliers, B. Agourram, E. B. Elabbassi and J. P. Libert, "A reproducible means of assessing the metabolic heat status of preterm neonates", *Med. Phys.*, Vol. 35, No. 1, pp. 89-100, (2008).

[8] A. Lubkowska, S. Szymanski and M. Chudecka, "Surface body temperature of full term healthy newborns immediately after birth – pilot study", *Int. J. Environ. Res. Public Health*, Vol. 16, No. 8, pp. 1-8, (2019).

[9] A. E. Wheldon, "Energy balance in the newborn baby: use of a manikin to estimate radiant and convective heat loss," *Phys. Med. Biol.*, Vol. 27, No. 2, pp. 285–296, (1982).

[10] T. Yamaguchi, T. W. Taylor, H. Okino, H. Horio and T. Hasegawa, "Computational fluid mechanical study of the convective heat transfer in a closed space simulating an infant incubator", *Front Med. Biol. Eng.*, Vol. 7, No. 2, pp. 129-141, (1996).

[11] M. K. Ginalski, A. J. Nowak and L. C. Wrobel, "Modelling of heat and mass transfer processes in neonatology", *Biomed. Mater.*, Vol. 3, No. 3, 034113, (2008).
[12] Y. H. Kim, C. H. Kwon and S. C. Yoo, "Experimental and numerical studies on convective heat transfer in a neonatal incubator", *Med. Biol. Eng. Comput*., Vol. 40, No. 1, pp. 114–121, (2002).
[13] M. K. Ginalski, A. J. Nowak and L. C. Wrobel, "A combined study of heat and mass transfer in an infant incubator with an overhead screen", *Med. Eng. Phys*., Vol. 29, No. 5, pp. 531–541, (2007).
[14] G. A. Ganesh, S. L. Sinha and T. N. Verma, "Numerical simulation for optimization of the indoor environment of an occupied office building using a double-panel and ventilation radiator", *J. Build. Eng.*, Vol. 29, pp. 101-139, (2019).
[15] G. A. Ganesh, S. L. Sinha and T. N. Verma, "Effect of inlet airflow direction on the indoor environment of naturally ventilated room using CFD", *Int. J. Eng. Adv. Technol.*, Vol. 9, No. 3, pp. 581-591, (2020).
[16] A. J. Chamkha, "On laminar hydromagnetic mixed convection flow in a vertical channel with symmetric and asymmetric wall heating conditions", *Int. J. Heat. Mass. Transfe.r*, Vol. 45, No. 12, pp. 2509–2525, (2002).
[17] A. J. Chamkha, "Unsteady laminar hydromagnetic fluid particle flow and heat transfer in channels and circular pipes", *Int. J. Heat. Fluid. Flow.*, Vol. 21, No. 6, pp. 740-746, (2000).
[18] D. C. Wilcox, "Formulation of the k-ω turbulence model revisited", *AIAA J.*, Vol. 46, No. 11, pp. 2823-2838, (2008).
[19] Star-CCM+ user's guide, release version 11.02, (2016).
[20] T. N. Verma, Numerical simulation of contaminant control in intensive care unit of hospitals, PhD Thesis, National Institute of Technology Raipur, India, accessed in Oct (2016).
[21] https://www.yankodesign.com accessed in Sept (2020).
[22] P. Decima, S. B. Erwan, A. Pelletier and L. Ghyselen, "Assessment of radiant temperature in a closed incubator", *Eur. J. Appl. Physiol.*, Vol. 112, No. 8, pp. 2957–2968, (2012).
[23] A. Hannouch, C. Habchi, T. Lemenand and K. Khoury, "Numerical evaluation of the convective and radiative heat transfer coefficients for preterm neonate body segments inside an incubator", *Build. Environ.*, Vol. 183, pp. 1070-85 (2020).
[24] J. H. Lienhard IV and J. H. Lienhard V, "*A Heat Transfer Textbook"*, 5th ed., Phlogiston Press Cambridge, Massachusetts, U.S.A., (2019).
[25] I. B. Celik, U. Ghia, P. J. Roache, C. J. Freitas, H. Coleman and P. E. Raad, "Procedure for estimation and reporting of uncertainty due to discretization in CFD Applications," *J. Fluids Eng.*, Vol. 130, No. 7, pp. 087001-4, (2008).
[26] K. Belghazi, E. B. Elabbassi, P. Tourneux, and J. P. Libert, "Assessment of whole body and regional evaporative heat loss coefficients in very premature infants using a thermal mannequin: Influence of air velocity", *Med. Phys.*, Vol. 32, No. 3, pp. 752–758, (2005).

How to cite this paper:

D. K. Baghel, S. L. Sinha and S. K. Dewangan, "SST K-ω based air flow and heat transfer assessment in an infant incubator", *J. Comput. Appl. Res. Mech. Eng.*, Vol. 12, No. 2, pp. 161-175, (2023).

DOI: 10.22061/JCARME.2022.7590.2010

URL: https://jcarme.sru.ac.ir/?_action=showPDF&article=1780